IEEE Access
Multidisciplinary | Rapid Review | Open Access Journal

Received 11 June 2023, accepted 25 June 2023, date of publication 10 July 2023, date of current version 20 July 2023.

Digital Object Identifier 10.1109/ACCESS.2023.3293889

APPLIED RESEARCH

Frequency Reconfigurable Beam Scanning Squarely Modulated Reactance Surface Antenna With Period and Surface Reactance Control

DOOHYUN YANG[1] AND SANGWOOK NAM[2], (Senior Member, IEEE)

[1]Samsung Electronics S.LSI Business, Hwasung 18279, South Korea

[2]College of Electrical and Computer Engineering, Institute of New Media Communication, Seoul National University, Seoul 08826, South Korea

Corresponding author: Sangwook Nam (snam@snu.ac.kr)

ABSTRACT In this study, a novel antenna design is proposed for designing a frequency-reconfigurable wide-angle beam scanning antenna and applied to a squarely modulated reactance surface leaky wave antenna. The antenna beam angle is electronically steered with discretely (rough beam scan) and continuously (precise beam scan) by controlling the antenna's modulation period and the surface reactance at any fixed frequency, respectively. The design procedure is provided for the squarely modulated reactance surface leaky wave antenna using unit cell composed of parallel microstrip conductors and varactors in between. The antenna's surface reactance is controlled by the DC bias voltages of the varactors. Based on the dispersion characteristic of the unit cell of the antenna, beam scanning states for different frequencies are designed. Although the operation frequency can be arbitrary, the model antenna is designed for the operation at two different frequencies of 4.6 and 5.8 GHz. It was implemented, and experimented for the demonstration of the proposed method. It is shown by an EM simulation that 72° and 91° of antenna beam scanning can be possible for 4.6 and 5.8 GHz bands, respectively. Also, some of the operational states (beams) are experimentally verified through utilizing DC bias voltages and a switching circuit. The numerical result and experimental result showed good agreement which verifies the proposed antenna design scheme.

INDEX TERMS Leaky-wave antennas (LWA), periodic structure, reconfigurable beam scanning antennas, surface reactance modulation.

I. INTRODUCTION

Recently, the necessity of the fixed frequency beam scanning antennas has been increased and some researches have been conducted to fulfill this requirement [1], [2], [3], [4], [5], [6], [7], [8], [9], [10], [11], [12]. Reconfigurability of the antennas are obtained using the tunable components such as p-i-n diodes and varactors [1], [2], [3], [4], [5] or with the materials like graphene [6], [7], liquid crystal [8], [9] and Barium Strontium Titanate (BST) [10], [11]. For the leaky wave antennas (LWAs), those reconfigurability methods are applied in order to control the periodicity of the antenna or the characteristic of the unit cell and fixed frequency beam scanning characteristic was obtained, overcoming the inherent frequency beam scanning characteristic [12]. Also, beam scanning including broadside radiation utilizing Chern photonic topological insulators has achieved [13].

The sinusoidally modulated reactance surface (SMRS) antenna, which is a type of a periodic leaky-wave antenna (LWA), is firstly proposed and analyzed by Oliner and Hessel [14] and researches on the electronic control of this type of the antenna are conducted [1], [2], [3], [4], [5], [6], [7], [8], [9], [14], [15], [16], [17], [18]. For the control of the reconfigurable SMRS antennas, two methods have been introduced; period control and surface reactance control. Period control method requires on/off control of the unit cell of the periodic structure and discretely tailors the floquet mode of the SMRS antenna for the control of the radiation characteristic [7]. On the other hand, surface reactance control method changes the surface reactance of the unit cell of the SMRS continuously in order to control the radiation characteristic of the SMRS antenna [1].

The associate editor coordinating the review of this manuscript and approving it for publication was Mohammad Zia Ur Rahman.

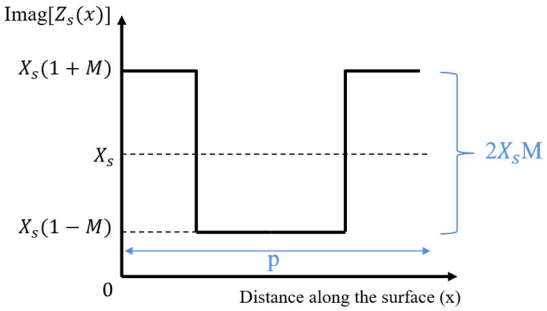

FIGURE 1. Unit period of the squarely modulated surface reactance profile expressed in equation (1).

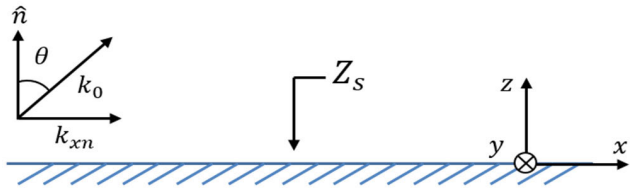

FIGURE 2. Wavenumber notation and surface reactance on periodically modulated reactance surface.

In this paper, we propose a frequency reconfigurable beam scanning squarely modulated reactance surface (SquMRS) antenna and applied the combined beam control methodology of the reconfigurable SMRS antenna which utilizes the advantages of the two control methods referred previously. Our proposed control method combines the control of the modulation period and the surface reactance of the SMRS antenna in order to achieve the delicate and wide beam-scanning characteristic and those parameters are controlled with the varactor diodes connected on the unit cell of the antenna and their DC bias voltages. Also, this design method allows the frequency reconfigurable beamscanning operation at multiple frequency bands. The beamscanning modes at different frequencies can be calculated based on the dispersion characteristic of the guided TM surface wave mode. $Z_s(x) =$ The reconfigurability and beam control methodology applied to our proposed antenna can control the radiating beam angles with more versatility along the multiple frequency bands when compared with the previously referred literatures.

II. THEORIES ON SMRS ANTENNA

When a guided wave propagates on a periodically modulated reactance surface, its spatial harmonics are generated and one of which is utilized as the main radiating mode of the periodic LWAs [14]. The term ''surface impedance'' is defined as the ratio of the tangential electric field to the tangential magnetic field of the guided surface wave; surface reactance is the imaginary part of this impedance. Among the various periodic surface reactance modulation profiles, we focused on the SquMRS profile because of its simplicity: it is composed either high or low surface reactance value, which enables simple reconfigurable beam scanning realization and control at fixed frequencies. In previous researches, the dispersion

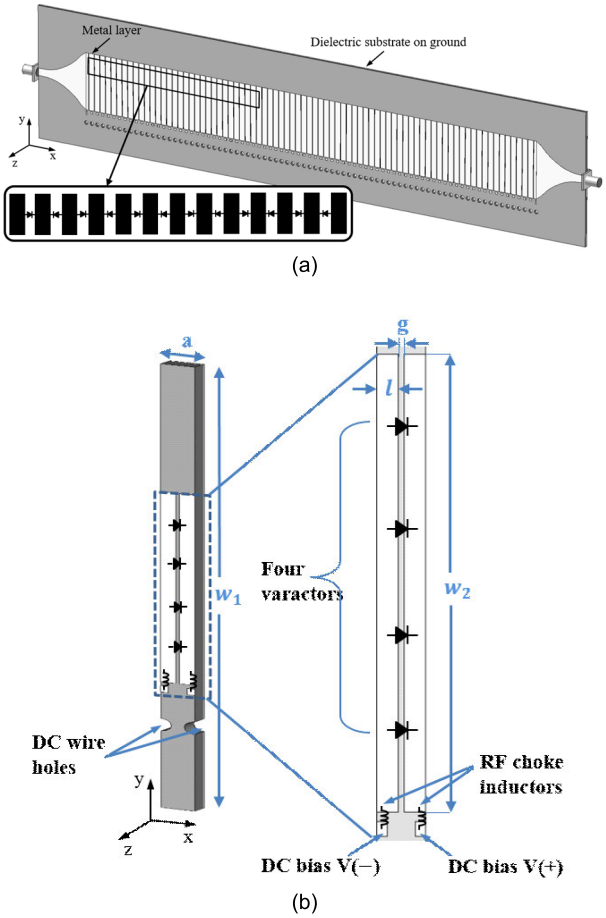

FIGURE 3. Configuration of proposed antenna structure and unit cell (a) Overall antenna structure (b) Unit cell's perspective view and enlarged top view. Structure parameters (mm): a = 3.2, g = 0.35, l = 1.425, w_1 = 70, w_2 = 30.

characteristics of the SquMRS and its application to the antenna have been analyzed [17], [18]. A squarely modulated reactance surface profile along the longitudinal direction (x-direction) can be expressed as

$$\begin{cases} jX_s(1+M) if\, 0 \le x \le p/4 \ or \ 3p/4 \le x \le p \\ jX_s(1-M) if p/4 < x < 3p/4 \end{cases} \quad (1)$$

where X_s is the average surface reactance, p is the modulation period and M is the modulation factor. The above equation can be plotted as shown in Fig.1. When a reactance surface is periodically modulated with this form, the dispersion characteristic of the guided wave was derived in previous researches [17], [18]. Spatial harmonics of the guided wave are generated according to the Floquet mode theory [19] and this geometry is graphically described in Fig. 2. The field's wavenumber in x-direction can be written as follows

$$k_{xn} = k_{x0} + 2\pi n/p \quad (2)$$

where k_{xn} and k_{x0} are the wavenumber of the n-th order Floquet harmonic and wavenumber of the fundamental mode in x-direction [15]. Among the various harmonics, -1st harmonic which is generally used as a main radiating mode for the

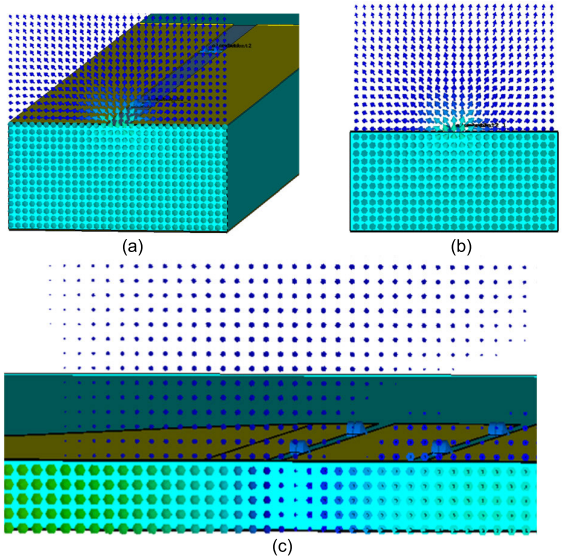

FIGURE 4. Simulated H-field distribution of unit cell and antenna at 5.8 GHz with XZ plane cut. (a) Perspective view of H-field distribution of the unit cell with eigenmode simulation. (b) Side view. (c) H-field distribution of the designed antenna with full EM simulation.

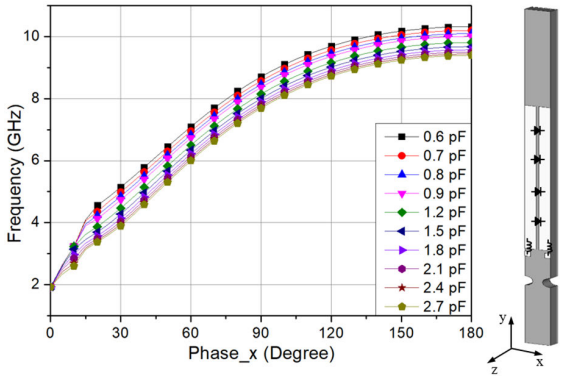

FIGURE 5. Dispersion curves of the TM surface wave on the unit cell according to different loading varactor capacitances and the configuration of the unit cell.

periodic LWAs is designed to generate leaky-wave radiation and its approximated phase constant (β_{-1}) and radiation angle (θ_{-1}) can be expressed with the parameters used in (1) as

$$\beta_{-1} = \beta_{approx} - 2\pi/p = k_0\sqrt{1+(X_s/\eta_0)^2} - 2\pi/p \quad (3)$$

$$\theta_{-1} = \arcsin(\sqrt{1+(X_s/\eta_0)^2} - 2\pi/k_0 p) \quad (4)$$

in which η_0 is the free-space wave impedance and k_0 is the free-space wavenumber. The phase constant of the fundamental mode (β_{-1}) is an approximated expression when the modulation amplitude M in (1) is assumed for small value and the exact expression is derived in [14] and [15].

III. CONFIGURATION OF THE PROPOSED ANTENNA AND UNIT CELL

The overall configuration of the antenna is depicted in Fig. 3(a). The antenna is composed of equally spaced

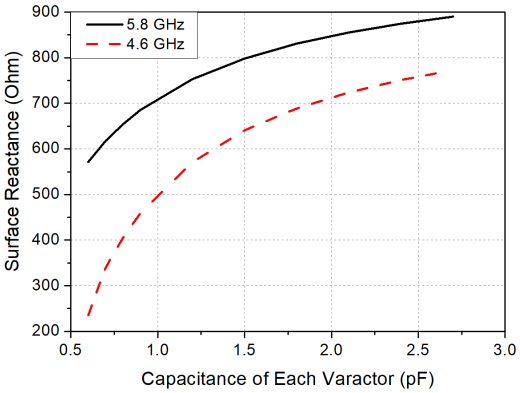

FIGURE 6. Surface reactance of the proposed antenna unit cell according to the loaded capacitance of each varactor at two different operation frequencies (4.6 and 5.8 GHz).

parallel microstrip conductors and varactors between them and tapered transition structures are placed at the input and output ports of the antenna. Overall antenna length including transition structures is 311 mm and this is about $4.7\lambda_0$ at 4.6 GHz and $6\lambda_0$ at 5.8 GHz of operation frequencies. Proposed antenna was designed with the TMM3 ($\varepsilon_r = 3.27, tan\delta = 0.002$) substrate which has 1.524mm of thickness. The unit cell structure of the proposed antenna is shown in Fig. 3(b) and detailed structure is described. In order to realize the reconfigurable squarely modulated reactance surface antenna, the unit cell of the antenna is composed of microstrip conductors and four varactors are loaded between the conductors. The varactor (Skyworks SMV2020-079LF) has the capacitance range of 0.35 pF to 3.2 pF. For the uniformity of the effective surface reactance profile within single unit cell, four varactors are loaded with equal distances instead of using single varactor at the middle of the conductors. The number of the varactors affects the amount of the capacitive loading within the unit cell. The width of the microstrip gratings (w_2) is determined based on the input matching of the proposed antenna. The capacitance between the conductors can be electronically controlled by the DC reverse bias voltage across the varactors. Enlarged figure shows the detailed structure of the unit cell and RF choke inductors (Murata LQW15AN11NG8ZD) with 11 nH of inductance and its pads are located below the microstrip conductors. DC bias voltages are supplied with wire through the hole structure. The overall structure of the proposed antenna is composed of 80 unit cells and total 320 of varactors are used for the antenna.

In order to analyze the surface wave mode utilized for the radiation of the antenna with the unit cell structure, its H-field distributions are plotted in Fig.4 (a) and (b). The H-field vector obtained from the eigenmode simulation of the unit cell at 5.8 GHz is normal to the XZ plane and this shows that the proposed unit cell structure supports TM surface wave mode as reported in other literature with same structure. The H-field distribution obtained from time domain simulation of the designed antenna structure (Fig.4(c)) showed same TM

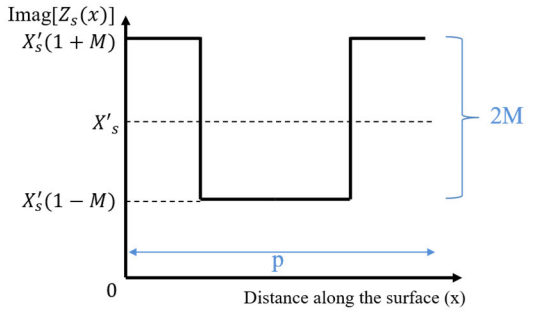

FIGURE 7. Unit period of average surface reactance controlled case of squarely modulated surface reactance profile with newly defined average surface reactance value X_s' from X_s of previous profile in Fig.1.

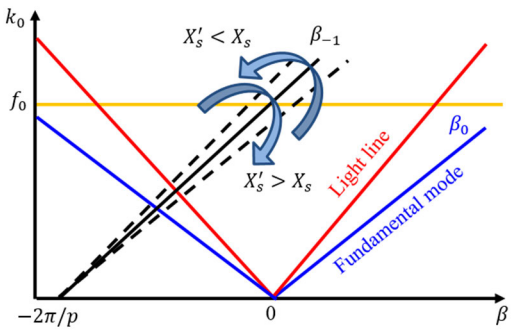

FIGURE 8. Description of the dispersion diagram of the proposed antenna when the average surface reactance is controlled (dashed black lines) from its original value (solid black line).

surface wave mode and this implies that our analyzed TM surface wave mode in eigenmode simulation is excited in full EM simulation.

Fig. 5 shows the dispersion curves of the TM surface wave mode supported on the unit cell. The dispersion curves are obtained from the eigenmode simulation according to the different varactor capacitances within the varactor capacitance range. The boundaries of the unit cell in the x-direction are adjusted as a periodic boundary condition and the simulation is conducted with the full-wave software, CST Microwave Studio. Considering the self-resonant frequency (6 GHz) of the RF choke inductor used for the unit cell, two frequencies (4.6 and 5.8 GHz) are determined to verify the proposed beam scanning methodology.

Fig. 6 shows the surface reactance range of the proposed antenna's single unit cell according to the loading capacitance of each varactor at 4.6 and 5.8 GHz. The surface reactance of the unit cell can be calculated by extracting wavenumber of unit cell along the propagation direction (x). The surface reactance of single unit cell can be calculated as follows

$$Z_s = j\eta_0\sqrt{(k_x/k_0)^2 - 1} \tag{5}$$

where k_x is the wavenumber in x direction [14]. Additional 0.29 pF of parasitic capacitance is incorporated in the designed lumped element model for the accuracy of the simulation which is verified in the datasheet of the varactor

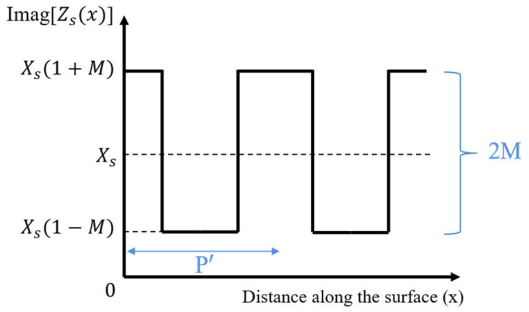

FIGURE 9. Surface reactance profile of period controlled case of squarely modulated surface reactance with newly defined period p' from p of previous profile in Fig.1.

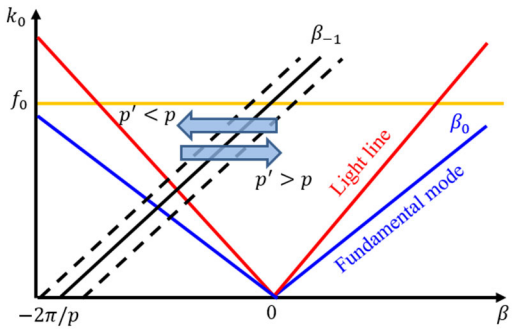

FIGURE 10. Description of the dispersion diagram of the proposed antenna when the modulation period is controlled (dashed black lines) from its original value (solid black line).

TABLE 1. Operation states of the designed antenna and Its parameters for Operation at 4.6 and 5.8 GHz.

Low Band Freq. (4.6 GHz)				High Band Freq. (5.8 GHz)		
Angle	No. of cells	X_s/η_0	State	X_s/η_0	No. of cells	Angle
-35.7°	9	1.35	1	1.8	6	-39°
-25.9°	10	1.25	2	1.95	6	-27°
-16°	11	1.2	3	1.8	7	-14°
-5.6°	12	1.25	4	1.85	8	5°
6.5°	13	1.35	5	1.9	9	20°
15°	14	1.4	6	1.95	10	35°
23°	15	1.45	7	1.9	11	42°
29°	16	1.45	8	1.9	12	53°
37°	17	1.5	9	N/A	N/A	N/A

manufacturer. Based on the simulated surface reactance range of the proposed antenna unit cell, two beam scanning schemes are applied and will be introduced in the next section.

IV. BEAM SCANNING SCHEME UTILIZING SURFACE REACTANCE AND MODULATION PERIOD CONTROL

For a periodically modulated SquMRS LWA, electronic control of the average surface reactance value (X_s) or the modulation period (p) allows the radiation beam control of the antenna at a fixed frequency. Effect of each parameter control is analyzed independently.

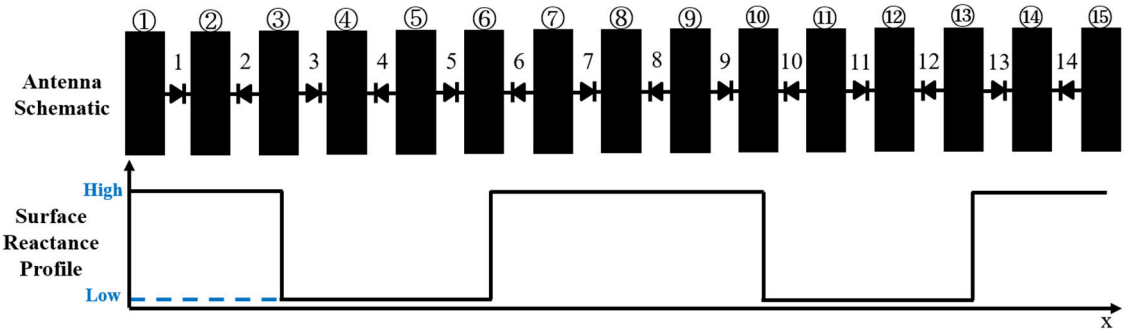

FIGURE 11. Antenna schematic with a single row arrangement of varactors(not scaled) and its squarely modulated reactance profile for State 3 operation at 5.8 GHz.

TABLE 2. Example of the antenna parameters for state 3 operation at 5.8 GHz.

Var. #	1	2	3	4	5	6	7	8	9	10	11	12	13	14
X_s	High 780.4Ω	High 780.4Ω	Low 576.8Ω	Low 576.8Ω	Low 576.8Ω	High 780.4Ω	High 780.4Ω	High 780.4Ω	High 780.4Ω	Low 576.8Ω	Low 576.8Ω	Low 576.8Ω	High 780.4Ω	High 780.4Ω
C_{var}	High 1.66 pF	High 1.66 pF	Low 0.9 pF	Low 0.9 pF	Low 0.9 pF	High 1.66 pF	High 1.66 pF	High 1.66 pF	High 1.66 pF	Low 0.9 pF	Low 0.9 pF	Low 0.9 pF	High 1.66 pF	High 1.66 pF
V_{rev}	2 V	2 V	13 V	13 V	13 V	2 V	2 V	2 V	2 V	13 V	13 V	13 V	2 V	2 V
Cond. #	①	②	③	④	⑤	⑥	⑦	⑧	⑨	⑩	⑪	⑫	⑬	⑭	⑮
V_{cond}	0 V	2 V	0 V	13V	0 V	13 V	11 V	13V	11 V	13 V	0 V	13 V	0 V	2 V	0 V

(Parameters in first column) **Var.#** : Varactor number, X_s : Surface reactance, C_{var} : Varactor capacitance, V_{rev} : Reverse bias voltage, **Cond.#** : Conductor number, V_{cond} : Conductor bias voltage.

A. AVERAGE SURFACE REACTANCE CONTROL

As already explained in literatures [14], [15], the dispersion curve of a periodically modulated reactance surface antenna can be approximated as a linear function. For a basic squarely modulated surface reactance profile shown in Fig. 1, average surface reactance control case from Fig. 1 is plotted as Fig. 7 and X_s' is the new average reactance value controlled from previous X_s. The control of the average surface reactance can be achieved within the allowable surface reactance range of the unit cell as shown in Fig. 5. This average surface reactance control leads to the manipulation of the main radiating -1st Floquet mode's slope as expressed in (3) and its concept can be described explicitly using dispersion diagram as shown in Fig. 8. If the radiating -1st Floquet mode of basic squarely modulated reactance surface profile shown Fig. 1 corresponds to the black solid line in Fig. 8, average surface reactance controlled curves can be plotted as black dashed lines at the sides of the solid curve by the approximated expression in (3). The slope of dashed lines are inversely proportional to the newly defined X_s'. This manipulation of the slope of the dispersion curve changes the crossing point with the constant frequency orange line (f_0) and this phase constant change at the operation frequency f_0 renders reconfigurable beam scanning of the proposed antenna at a fixed frequency. As the surface reactance of the unit cell can be adjusted continuously according to the bias voltage of the varactor, beam scanning of the antenna can be achieved continuously within the controllable surface reactance range of the unit cell.

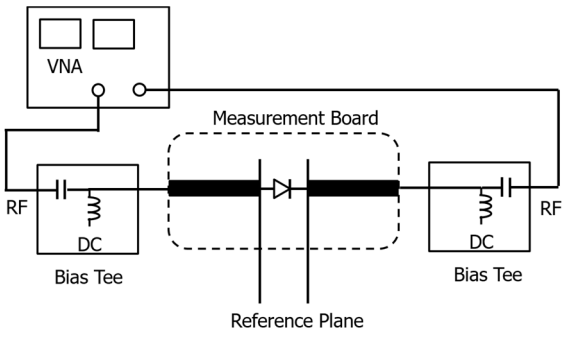

FIGURE 12. Experimental environment for the TRL de-embedding of varactor diode used in the design of the proposed antenna.

B. MODULATION PERIOD CONTROL

When the modulation period is controlled from the basic squarely modulated reactance surface form in Fig. 1, its profile can be depicted as shown in Fig. 9, where p' is the new period changed from previous p of Fig. 1. In this case, the second term in the right hand side of (3) is dependent on the modulation period and the phase constant of radiating -1st Floquet mode can be adjusted at a fixed frequency. This effect is graphically illustrated in Fig. 10. The second term

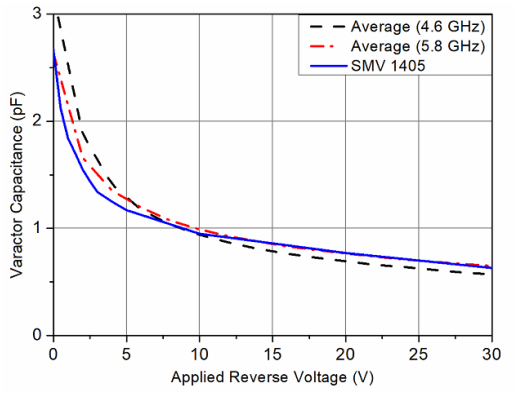

FIGURE 13. Plot of the extracted capacitance of the varactor with the experimental setup in Fig. 12 measured at 4.6 GHz (Dashed) and 5.8 GHz (Dashed dot) and compared with the capacitance value verified in the datasheet (Solid).

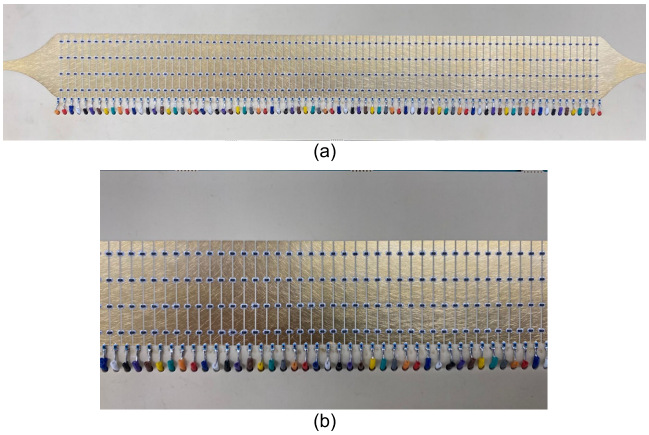

FIGURE 14. Fabricated sample of the designed antenna. (a) Overall structure. (b) Enlarged part of the antenna.

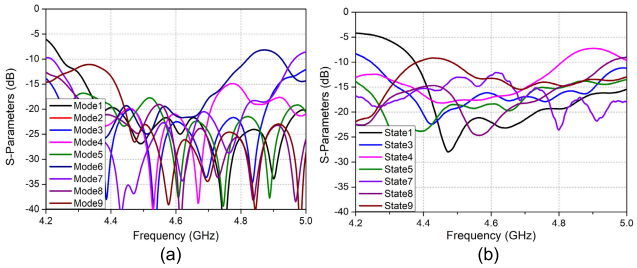

FIGURE 15. S-parameters of the designed antenna for the operation at 4.6 GHz (a) Simulated S_{11} of nine operation states. (b) Measured S_{11} of seven states.

in the right hand side of (3) corresponds to the x-abscissa of the dispersion curve of radiating -1st Floquet mode. So the control of the modulation period leads to the shift of the black solid dispersion curve in x-direction as plotted in dashed black curves and the shift direction is determined by whether the modulation period is lengthened or shortened. The longer period moves the curve closer to the origin and the shorter period makes the curve farther from the origin. Crossing point of the constant frequency orange line (f_0) and dispersion curve can be changed due to the control of modulation period which means reconfigurable control of phase constant and this enables the beam scanning of the proposed antenna at a fixed frequency f_0. The modulation period control has discrete beam scanning characteristic as the modulation period increases with the multiple of the unit cell (a in Fig. 3(b)) size, this makes the dispersion curve in Fig. 10 shifts discretely according to different modulation periods with the relation of equation (2).

V. ANTENNA DESIGN

Combining the two beam scanning schemes introduced in the previous section, a frequency reconfigurable beam scanning SquMRS antenna at a fixed frequency is designed. As mentioned earlier, two frequencies (4.6 and 5.8 GHz) are determined for the frequency reconfigurable beam scanning operation and these two frequencies are determined considering the self-resonance frequency of the inductor (6 GHz) used as a RF choke.

A. BEAM SCANNING STATES OF THE DESIGNED ANTENNA

With the obtained surface reactance range of the proposed antenna unit cell in Fig. 6, normalized surface reactance (X_s/η_0) values of 1.35 (508.9 Ω) to 1.5 (565.5 Ω) for 4.6 GHz and 1.8 (678.6 Ω) to 1.95 (735.15 Ω) for 5.8 GHz are utilized for the average surface reactance controlled beam scanning. Those values are determined with some margin for the design of the antenna and the region whose surface reactance is highly dependent on the capacitor value has avoided. Period control of the squarely modulated reactance surface is achieved by changing the number of the unit cells which are composing single period of modulated reactance surface. The period of the periodically modulated reactance surface is determined within the periodicity condition for the periodic leaky wave antenna ($p > \lambda_g/2$).

The designed antenna's operation modes and parameters for 4.6 and 5.8 GHz including calculated angles are summarized in Table 1. Beam scanning states are designed so that can cover some range from backward to forward beams within the range that the antenna performance is not that deteriorated. Low band operation (4.6 GHz) and the high band operation (5.8 GHz) are designed with 9 and 8 states for each. Each state is composed of different normalized surface reactance values and unit cells in order to cover the beam scanning range. Radiation angle of each operation state is calculated utilizing equation (4). Modulation amplitude M is determined with 0.15 for all operation states.

B. BEAM SCANNING OPERATION EXAMPLE

Figure 11 shows the schematic of the designed beam scanning antenna and its surface reactance profile along the antenna length direction (x). State 3 of 5.8 GHz operation in Table 1 is chosen as an example of the operation state and the part of the antenna schematic and its surface reactance profile in x-direction are described. The vertical lines stand for the microstrip conductors and the varactors are placed between the conductors and only single varactor is presented between

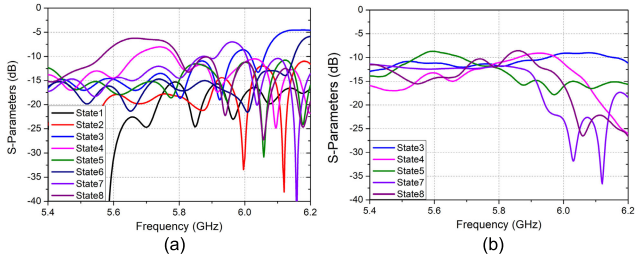

FIGURE 16. S-parameters of the designed antenna for the operation at 5.8 GHz (a) Simulated S_{11} of eight operation states. (b) Measured S_{11} of five states.

TABLE 3. Surface reactance control beam scanning state results at 5.8 GHz.

Normalized Surface Reactance	Calculated Angle	Simulated Angle	Measured Angle
X_s/η_0=1.8	14°	12°	13°
X_s/η_0=1.875	18°	16°	18°
X_s/η_0=1.95	22°	19°	21°

the conductors for the simplicity. The direction of the varactors are alternatingly loaded in order to prevent progressive increase of DC bias voltage and keep the minimal number of different DC bias voltages. When the varactors are loaded with same direction, it will require more than eighty different DC bias voltages in real structure because the overall antenna structure is composed of eighty unit cells. Table 2 shows the surface reactance, varactor capacitance and DC reverse bias voltages for the varactors in case of State 3 of the Table 1. As the State 3 of the 5.8 GHz operation of the antenna is composed of seven unit cells in a surface reactance modulation period, each parameter's state changes repeatedly with seven unit cells of period. The exact values of the parameters are calculated from the average surface reactance (X_s) and modulation amplitude (M) of the state. In case of State 3, normalized surface reactance is 1.8 and has 0.15 of modulation amplitude, high value of surface reactance requires 780.4Ω and 576.8Ω for low value. Required loading capacitances according to the surface reactance values can be extracted from data in Fig. 5 and then required DC reverse bias voltage for varactors are determined. Conductor numbers and their bias in Table 2 are going to be discussed in section VI.

VI. EXPERIMENTAL RESULTS

For the realization and measurement of the proposed squarely modulated reactance surface antenna, detailed implementation process and its measurement procedure are introduced and its results are provided.

A. VARACTOR CHARACTERIZATION

Prior to the measurement of the designed antenna, characterization of the varactor diode which is used for the design of the antenna was conducted with TRL (Thru Reflect Line) de-embedding method [20]. The capacitances of the varactor

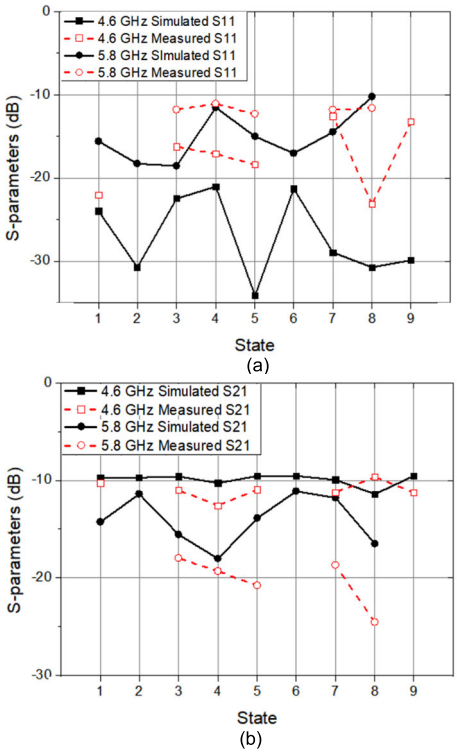

FIGURE 17. Simulated and measured S11 of the designed antenna according to the operation states at 4.6 GHz and 5.8 GHz (a) and S21 of the designed antenna (b).

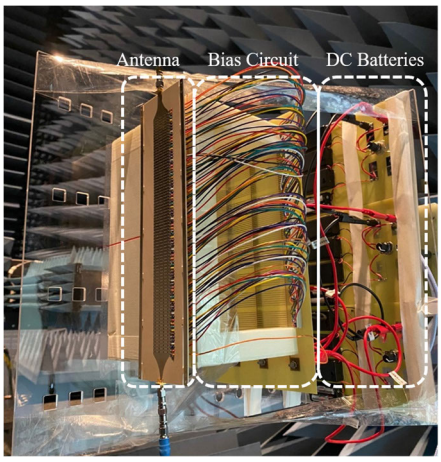

FIGURE 18. Pattern measurement setup of the implemented antenna. Each part of the antenna system is described and assembled on an acrylic jig.

according to the DC reverse bias voltages at the 4.6 GHz and 5.8 GHz frequency are extracted. Experimental environment for the TRL de-embedding of the varactor is shown in Fig. 12. After the measurement of the DUT measurement board (FR-4), line effects are de-embedded with the measurement of the Thru, Reflect, and Line measurement board in order to obtain the series impedance of the varactor diode at the reference plane which corresponds to the B parameter of the ABCD matrix. Then the capacitance of the varactor is calculated considering the operation frequency.

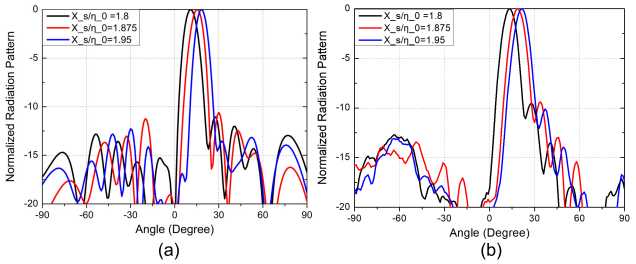

FIGURE 19. Radiation patterns of the average surface reactance control beam scanning modes at a 5.8 GHz of operation frequency. (a) Simulated radiation patterns. (b) Measured radiation patterns.

Two sample varactors are measured and averaged result of the varactor capacitance according to the DC revers bias is shown in Fig. 13. The solid line shows the data provided from the varactor manufacturer and dashed line shows the averaged measured result at 4.6 GHz. The dashed dot line is the averaged result at 5.8 GHz. Extracted results showed slight difference when compared with the provided data from datasheet and the difference was higher in low bias voltage region. Also, the parasitic resistance of the varactor was measured to be 2.4Ω, which is higher than the value (0.8Ω) verified in the datasheet of the varactor manufacturer. Antenna experiment is conducted based on the obtained varactor characteristic and DC reverse bias voltages are determined for the antenna operation.

B. BS-PARAMETER RESULTS

Proposed antenna structure shown in Fig. 3(a) is fabricated and its overall structure is shown in Fig. 14(a). As described previously, four varactors are loaded between the conductor lines and share the same DC bias voltage supplied at the bottom tip of the conductor as shown in Fig. 14(b). The bottom tips of the conductor lines are connected with DC bias wires through the RF choke inductor. Only four independent DC bias voltages were available for the measurement of the antenna operation due to the realization of the portable battery circuit.

Before showing the measurement result, we notify that due to the finite number of available DC voltages, part of the operation states for 4.6 GHz and 5.8 GHz are measured. For low band operation states (4.6 GHz), State 1, 3, 4, 5, 7, 8 and 9 are measured and State 3, 4, 5, 7 and 8 are measured for high band operation states (5.8 GHz). Other operation states which could not be measured require additional DC bias voltages more than four as the surface reactance profile repeats. This is determined from the number of unit cell composing a period of surface reactance profile. One of the bias example for the State 3 is shown in lower part of the Table 2 and it requires four different DC bias voltages with shown two periods of the surface reactance profile and the number of the required DC bias voltages is just the same as the period repeats. Bias voltages for conductors are determined from the bias voltages for the varactor reverse bias voltages calculated from its SquMRS parameters.

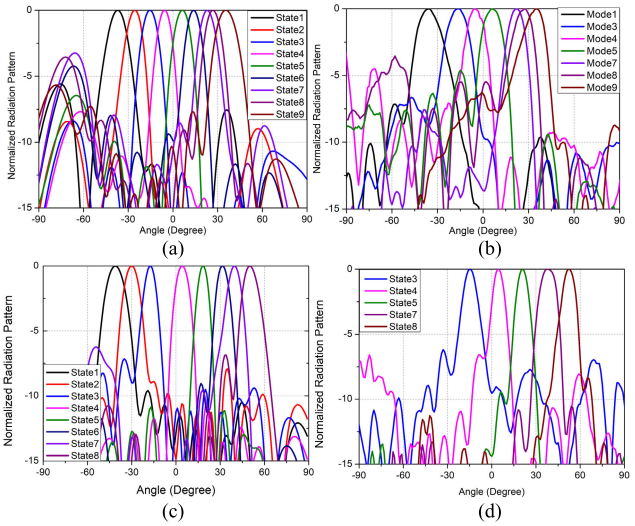

FIGURE 20. Radiation patterns of the proposed antenna. (a) Simulated patterns of the nine operation states at 4.6 GHz. (b) Measured patterns of the seven operation states at 4.6 GHz. (c) Simulated patterns of the eight operation states at 5.8 GHz. (d) Measured patterns of the five operation states at 5.8 GHz.

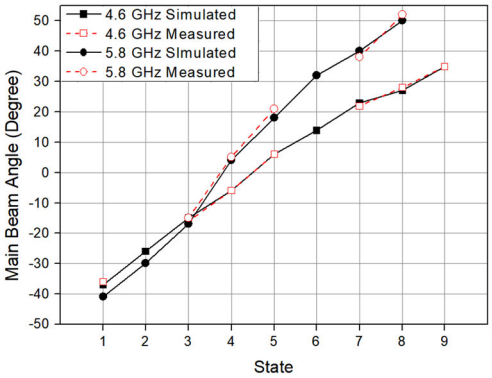

FIGURE 21. Simulated and measured beam scanning angle of the designed antenna at 4.6 GHz and 5.8 GHz according to the operation.

Simulated and measured reflection coefficient of the designed antenna at 4.6 GHz and 5.8 GHz are shown in Fig. 15 and 16 respectively, and the values at each operation frequency according to operation states are plotted in Fig. 17(a). All the states at each operation frequency show lower than -10 dB. For state 4 which is close to the broadside radiation, does not show open-stopband effect even though any matching technique [21] did not apply for the proposed antenna. This is due to the high loss from the parasitic resistance of the varactor utilized for the design. Large number of varactors caused high accumulation of the loss and this lead to the suppression of the open-stopband effect which is already discussed in [1]. This is also observed in pattern measurements and to be discussed in next section. Simulated and measured S_{21} are also plotted in Fig. 17(b) at each operation frequency. Measured results show lower level of S_{21} when compared with the simulated results. This is caused from higher loss component of the varactor diode whose de-embedded series resistance is measured about 2.4Ω

TABLE 4. Comparison of the proposed antenna and reported beam scanning modulated reactance surface antennas.

Ref	Reconfigurability method	Beam scanning scheme	Operation band	Antenna length	3 dB scanning range		Peak gain (dBi)	
					Simulated	Measured	Simulated	Measured
[1]	Varactor diode	Surface reactance control	Single	$6\sim6.4\lambda_0$	N/A	45°	N/A	8
[2]	Varactor diode	Surface reactance control	Multi (Dual)	$4.65\lambda_{01}$ & $7.17\lambda_{02}$	62° & 9°	80° & 22° (Not 3dB)	13(Realized) & 14(Realized)	6 & 7
[5]	Graphene	Surface reactance control	Single	$2.13\lambda_0$	45° (not 3dB)	N/A	6.6	N/A
[6]	Graphene	Period control	Single	$1.74\lambda_0$	45°	N/A	N/A	N/A
This work	Varactor diode	Surface reactance control + Period control	Reconfigurable	$4.7\lambda_{01}$ & $6\lambda_{02}$	72° & 91°	73° & 67° (Part of modes)	6 & 7.53	5 & 5.62

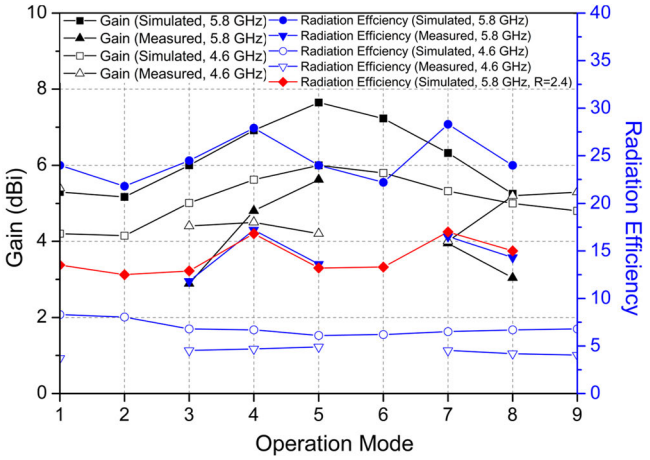

FIGURE 22. Simulated and measured gain and radiation efficiency of the for 4.6 GHz and 5.8 GHz.

from the varactor characterization which is higher than 0.8Ω of parasitic resistance provided in the varactor datasheet. De-embedded series resistance of the varactor include additional substrate loss caused from the measurement board (FR-4) but still have higher loss resistance when compared with value verified in the datasheet and this affected the low level of measured S_{21} result.

C. PATTERN MEASUREMENT RESULTS

Fig. 18 shows the measurement setup for the radiation pattern of the implemented antenna. Overall system required for the antenna operation is assembled on an acrylic jig. Firstly, average surface reactance control beam scanning result is shown in Fig. 19. Three operation states with different average surface reactance values (X_s/η_0 =1.8, 1.875 and 1.95) but the same number of unit cells within a modulation period are simulated and measured. These states are based on 9 unit cells in a modulation period like State 5 in Table 1. Fig. 19(a) and 18(b) show the simulated and measured result of the beam scanning and normalized radiation patterns of each state are plotted. Radiation angles for each cases in Fig. 19 is arranged in Table 3. Slight differences between calculated, simulated and measured radiation angles are observed but the discrepancies are within few degrees.

Radiation patterns of the operation states shown in Table 1 are plotted in Fig. 20. Simulated nine beam scanning states are shown in Fig. 20(a) at 4.6 GHz and measured five states (State 1, 3, 4, 5, 7, 8 and 9) are shown in Fig. 20(b). Simulated and measured pattern results at 5.8 GHz are plotted in Fig. 20(c) and 20(d). Simulated eight states and measured five states are plotted in each figure. As the antenna beam angle scans from left to right, the radiation pattern shows higher sidelobe level on the left side of the main beam, which is originated from the $n = -2$ Floquet harmonic radiation. Radiation angles for each operation frequencies according to the states are plotted in Fig. 21. About 72° and 91° of beam scanning ranges are obtained for 4.6 GHz and 5.8 GHz from simulated result. Part of the operation states are measured and those results validates the proposed beam scanning scheme with good agreement when compared with the simulated values.

The antenna gain and efficiency according to operation states are shown in Fig. 22. For the low frequency (4.6 GHz), the simulated gain varies within a range of 4 to 6 dBi and the simulated efficiency ranges between 6% and 8%. The high frequency (5.8 GHz) results show that the gain ranges from 5 to 7.5 dBi and the simulated efficiency from 21% to 27.5% for this case. Measured results at 4.6 GHz showed a gain range from 4 to 5 dBi, while obtaining a radiation efficiency of approximately 5 %. Measured result at 5.8 GHz showed a gain range from 3 to 5.8 dBi and an efficiency range of 12% to 17 %. As can be expected from the measured S_{21} result, the measured gain and efficiency are lower for both frequencies when compared with the simulated value. Diamond symbol graph in Fig. 21 shows the simulated radiation efficiency at 5.8 GHz when the varactor loss component is considered as 2.4 Ω, which shows good agreement with the measured radiation efficiency and supports our varactor characterization result.

Table 4 summarizes the results obtained with the proposed antenna and the results of the reported beam scanning modulated reactance antennas. This comparison shows that the proposed antenna exhibits a wider scanning range and competent gain considering its relative size when compared with previous single band beam scanning studies. In addition, the

proposed antenna achieved a well-balanced beam scanning range for low- and high- band operations when compared with the multi-band beam scanning antenna in the literature, which shows the validity of the proposed beam scanning methodology for the multi-band beam scanning operation of the modulated reactance surface antenna.

VII. CONCLUSION

In this paper, we proposed a frequency reconfigurable beam scanning LWA which is based on an electronically controllable SquMRS. Proposed antenna's unit cell is composed of microstrip conductors and varactors loaded between the conductors whose capacitance is electronically controlled with the DC bias voltage. Average surface reactance value control allows continuous beam scanning while surface reactance modulation period control leads to the discrete beam scanning. It was shown the combination of two beam scanning schemes can achieve the frequency reconfigurable beam scanning. Calculated and simulated result of beam scanning states are shown and part of the beam scanning states are verified with the measurement result and those results showed good agreement. About 72° and 91° of beam scanning ranges are obtained for low and high frequency operation and the measured gain was 5 dBi and 5.62 dBi. The gain values are degraded from the simulated result due to the higher varactor loss than expected. However, better performance is expected when the low loss varactor is used or the reconfigurability is achieved with the other reconfigurable materials. The novelty of the proposed antenna is in the proposal of the combination of two beam scanning schemes of periodically modulated reactance surface antennas with frequency reconfigurability beam scanning property based on the dispersion characteristic of the unit cell.

REFERENCES

[1] M. Wang, H. F. Ma, H. C. Zhang, W. X. Tang, X. R. Zhang, and T. J. Cui, "Frequency-fixed beam-scanning leaky-wave antenna using electronically controllable corrugated microstrip line," *IEEE Trans. Antennas Propag.*, vol. 66, no. 9, pp. 4449–4457, Sep. 2018.

[2] M. Wang, H. F. Ma, W. X. Tang, H. C. Zhang, W. X. Jiang, and T. J. Cui, "A dual-band electronic-scanning leaky-wave antenna based on a corrugated microstrip line," *IEEE Trans. Antennas Propag.*, vol. 67, no. 5, pp. 3433–3438, May 2019.

[3] Z. Li, Y. J. Guo, S. Chen, and J. Wang, "A period-reconfigurable leaky-wave antenna with fixed-frequency and wide-angle beam scanning," *IEEE Trans. Antennas Propag.*, vol. 67, no. 6, pp. 3720–3732, Jun. 2019.

[4] S. Wang, Z. Li, M. Chen, and J. Wang, "Dual-band fixed-frequency beam-scanning leaky-wave antenna for large-frequency-ratio microwave and millimeter-wave applications," *IEEE Trans. Antennas Propag.*, vol. 70, no. 9, pp. 7458–7467, Sep. 2022.

[5] A. H. Panaretos and D. H. Werner, "Leaky-wave antennas based on capacitively tuned modulated reactance surfaces," *IEEE Antennas Wireless Propag. Lett.*, vol. 15, pp. 678–681, 2016.

[6] Y. Cheng, L. Wu, M. Tang, Y. Zhang, and J. Mao, "A sinusoidally-modulated leaky-wave antenna with gapped graphene ribbons," *IEEE Antennas Wireless Propag. Lett.*, vol. 16, pp. 3000–3004, 2017.

[7] M. Esquius-Morote, J. S. Gómez-Díaz, and J. Perruisseau-Carrier, "Sinusoidally modulated graphene leaky-wave antenna for electronic beamscanning at THz," *IEEE Trans. THz Sci. Technol.*, vol. 4, no. 1, pp. 116–122, Jan. 2014.

[8] S. C. Pavone, E. Martini, F. Caminita, M. Albani, and S. Maci, "Surface wave dispersion for a tunable grounded liquid crystal substrate without and with metasurface on top," *IEEE Trans. Antennas Propag.*, vol. 65, no. 7, pp. 3540–3548, Jul. 2017.

[9] H. Kim and S. Nam, "Performance improvement of LC-based beam-steering leaky-wave holographic antenna using decoupling structure," *IEEE Trans. Antennas Propag.*, vol. 70, no. 4, pp. 2431–2438, Apr. 2022.

[10] K. K. Karnati, M. E. Trampler, and X. Gong, "A monolithically BST-integrated Ka-band beamsteerable reflectarray antenna," *IEEE Trans. Antennas Propag.*, vol. 65, no. 1, pp. 159–166, Jan. 2017.

[11] K. K. Karnati, Y. Shen, M. E. Trampler, S. Ebadi, P. F. Wahid, and X. Gong, "A BST-integrated capacitively loaded patch for Ka-band and X-band beamsteerable reflectarray antennas in satellite communications," *IEEE Trans. Antennas Propag.*, vol. 63, no. 4, pp. 159–166, Apr. 2015.

[12] C. Walter, *Traveling Wave Antennas*. New York, NY, USA: McGraw-Hill, 1965.

[13] Z. Xu, M. Wang, S. Fang, H. Liu, Z. Wang, and D. F. Sievenpiper, "Broadside radiation from Chern photonic topological insulators," *IEEE Trans. Antennas Propag.*, vol. 70, no. 3, pp. 2358–2363, Mar. 2022.

[14] A. Oliner and A. Hessel, "Guided waves on sinusoidally-modulated reactance surfaces," *IRE Trans. Antennas Propag.*, vol. 7, no. 5, pp. 201–208, Dec. 1959.

[15] A. M. Patel and A. Grbic, "A printed leaky-wave antenna based on a sinusoidally-modulated reactance surface," *IEEE Trans. Antennas Propag.*, vol. 59, no. 6, pp. 2087–2096, Jun. 2011.

[16] D. Yang and S. Nam, "Tapered unit cell control of a sinusoidally modulated reactance surface antenna," *IEEE Antennas Wireless Propag. Lett.*, vol. 17, no. 12, pp. 2479–2483, Dec. 2018.

[17] M. Casaletti, "Guided waves on scalar and tensorial reactance surfaces modulated by periodic functions: A circuital approach," *IEEE Access*, vol. 7, pp. 68823–68836, 2019.

[18] H. Yu, K. Zhang, X. Ding, and Q. Wu, "A dual-beam leaky-wave antenna based on squarely modulated reactance surface," *Appl. Sci.*, vol. 10, no. 3, p. 962, Feb. 2020.

[19] A. K. Bhattacharyya, *Phased Array Antennas: Floquet Analysis, Synthesis, BFNs and Active Array Systems*. Hoboken, NJ, USA: Wiley, 2006.

[20] D. M. Pozar, *Microwave Engineering*, 4th ed. Hoboken, NJ, USA: Wiley, 2005.

[21] S. Paulotto, P. Baccarelli, F. Frezza, and D. R. Jackson, "A novel technique for open-stopband suppression in 1-D periodic printed leaky-wave antennas," *IEEE Trans. Antennas Propag.*, vol. 57, no. 7, pp. 1894–1906, Jul. 2009.

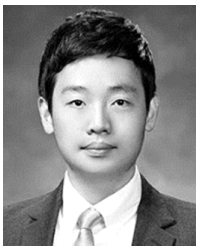

DOOHYUN YANG received the B.S. degree in electrical and electronic engineering from Chung-Ang University, Seoul, South Korea, in 2014, and the Ph.D. degree in electrical engineering and computer science from Seoul National University, Seoul, in 2021.

Since 2021, he has been a NR 5G Antenna and System Designer with Samsung Electronics S.LSI Business. His research interests include leaky wave antennas and metamaterial-based antennas and reconfigurable beam-scanning antennas.

SANGWOOK NAM (Senior Member, IEEE) received the B.S. degree in electrical engineering from Seoul National University, Seoul, South Korea, in 1981, the M.S. degree in electrical engineering from the Korea Advanced Institute of Science and Technology (KAIST), Seoul, in 1983, and the Ph.D. degree in electrical engineering from The University of Texas at Austin, Austin, TX, USA, in 1989. From 1983 to 1986, he was a Researcher with the Gold Star Central Research Laboratory, Seoul. Since 1990, he has been a Professor with the School of Electrical Engineering and Computer Science, Seoul National University. His research interests include the analysis/design of electromagnetic structures, antennas, and microwave active/passive circuits.